Multiple ion dynamics model for the collisionless rf sheaths and the ion energy distributions at rf-biased electrodes in fluorocarbon plasmas

Zhong-Ling Dai* and You-Nian Wang
The State Key Laboratory of Materials Modification by Laser, Electron, and Ion Beams, Department of Physics, Dalian University of Technology, Dalian 116023, People's Republic of China
(Received 20 December 2001; revised manuscript received 14 May 2002; published 26 August 2002)

With a one-dimensional multiple ion dynamics model, we study characteristics of the collisionless radio-frequency (rf) sheaths in fluorocarbon plasmas and calculate the ion energy distributions impinging on rf-biased electrodes. All the time-dependent terms in the ion fluid equations are included and the relationship between the instantaneous sheath voltage and sheath thickness is determined self-consistently by an equivalent circuit equation. The numerical results show that, due to the existence of multi-ion species, the sheath structure in the present work is different from those of single-ion species plasmas, and multiple peaks appear in the ion energy distributions. It is also shown that some parameters such as the bias frequency, bias power, bulk plasma density, and electron temperature are crucial for determining the shape of the ion energy distribution in multicomponent plasmas.

DOI: 10.1103/PhysRevE.66.026413 PACS number(s): 52.65.−y, 52.40.Hf

I. INTRODUCTION

In recent years, there has been a growing interest in using low pressure, high density plasmas in the microelectronics industry for fabrication of the new generation ultra-large-scale integrated circuits. Especially, these kinds of plasma are frequently used for anisotropic etching of semiconductor, oxide, and metal surfaces. It is well known that the ion energy and angular distributions (IEDs and IADs) arriving at wafers are crucial in determining the etch rates, etch profiles, and selectivity to different materials. Generally, the wafers are usually rested on a radio-frequency (rf) biased electrode in the etching process. The IEDs and IADs bombarding the electrode can be controlled by the rf sheath that is formed near the surface of the electrode.

In order to accurately predict the IEDs and IADs, it is important to investigate the characteristics of rf sheaths with multicomponent plasmas. Over the past decades, the characteristics of the rf sheath with single-ion species plasmas are well described by various theoretical models [1–14]. A critical parameter for determining the rf sheath dynamics is the ratio $\beta=\omega/\omega_{pi}$, where ω is the rf bias frequency and ω_{pi} is the ion plasma frequency for the single-ion species plasma. In the low-frequency range ($\beta\ll 1$), the ions traverse the sheath in a short time compared to the rf cycle and respond to an instantaneous sheath potential, which is because ion inertia dose not stop it instantaneously adjusting to the slowly varying field. In this case, the sheath can be described as a series of direct-current (dc) sheaths at the different moments in the time during the rf cycle. In the high-frequency range ($\beta\gg 1$), however, the ions experience many rf field oscillations while in the transit through the sheath and respond to a time-averaged sheath potential instead of the instantaneous sheath potential. Thus, the sheath dynamics can be simplified by neglecting all time-dependent terms in the ion fluid equations. The most difficult situation is in the intermediate frequency range when $\beta\sim 1$, because in the case the ion inertia allows it to only partially respond to the time-varying fields in the sheath. Most recently, a self-consistent rf sheath model was proposed, which includes all time-dependent terms in ion fluid equations and comprise an equivalent circuit model to determine the relationship between the instantaneous potential at a rf-biased electrode and sheath thickness [14]. Meanwhile, the characteristics of the IEDs with single-ion species plasmas have also been studied both theoretically and experimentally [9,14–19,29–31]. In particular, it has been found that the IEDs have bimodal shapes in the low- and intermediate-frequency range [9,14–19,29–31].

For the plasma etching processes, the etching rate and quality depend on not only the ion energy incident onto the substrates, but also the feedstock gas composition and the kind of gas discharge used. In practice, high density C_4F_8/Ar plasmas are commonly used for etching the oxide film of silicon in order to enhance the selectivity and etch rates, in which there are positive ions such as Ar^+, CF^+, CF_2^+, CF_3^+ and negative ions such as F^-. The experimental measurements of IEDs performed by Kuypers and Hopman [20] with low pressure argon, oxygen and fluorocarbon discharges driven by 13.56 MHz have demonstrated that the IEDs of multicomponent plasmas are bimodal as those of single species gas rf discharges, but a notable effect is that there are some splits in the peaks of the IEDs, which may reveal that different kind of positive ion with different ion mass has its own ion energy distribution incident onto the rf-biased electrode. Edelberg *et al.* [21] also found similar phenomenon in Ar/Ne and CF_4/O_2 discharges. On the aspect of theories, Sarma *et al.* [22] found that the sheath structure in a multicomponent plasma with negative ions follows the modified Child law in a dc sheath. Additionally, with the particle simulation code, Hrach and Hrachova [23] studied the influence of negative ions on plasma properties under a dc positive bias voltage condition in an O_2/Ar plasma. Considering two

*Email address: daizhl@dlut.edu.cn

 ©2002 The American Physical Society

kinds of positive ions N_2^+ and N^+, Kim [24] simulated the evolution of a sheath when a high negative voltage pulse was applied to the target in the plasma source ion implantation process. The numerical method of Midha and Economou [25] described the dynamics of ion-ion plasmas under a rf bias in which there were no electrons and negative ions. Recently, Ostrikov *et al.* [26] have proposed a numerical model for fluorocarbon plasmas with negative ions in near-electrode regions. But in this model a dc negative bias voltage was applied to the electrode rather than a rf bias. As far as know, the self-consistent model of rf sheaths and the simulation of the IEDs with multicomponent plasmas have not been proposed so far.

In this paper, we extend our previous work [14] and present a self-consistent dynamics model to describe collisionless rf sheaths with multicomponent plasmas, such as C_4F_8/Ar plasmas. The model includes all the time-dependent terms in the ion fluid equations and the time-variation capacitance term in the equivalent circuit model. This paper is outlined as follows. In Sec. II the basic model is described, including the ion fluid equations, equivalent circuit model, boundary conditions, and formula for calculating the IEDs of multicomponent plasmas. Then, in Sec. III, we present some numerical solutions of the rf sheath and show the time-dependent voltage wave form, sheath thickness, and spatiotemporal variations of densities for all kinds of particle. Also, making use of the model, the ion energy distributions bombarding rf-biased electrodes are determined numerically for the C_4F_8/Ar discharges. Finally, a short summary is given in Sec. IV.

II. MODEL DESCRIPTION

In the experiments on highly selective poly-silicon etching, the gas mixtures of octafluorocyclobutane (e-C_4F_8) and argon [27] are composed of electrons, positive ions Ar^+, CF^+, CF_2^+, and CF_3^+, as well as negative F^- ions, whereas other ions, such as C_xF_y $(x>1)$, C_x^+, and F^+, can be negligible. According to the actual experiment, in 90% Ar and 10% C_4F_8 gas mixtures at 20 mTorr, the ion number densities satisfy $n_{CF^+}>n_{CF_2^+}>n_{CF_3^+}$, and the proportion of argon ions varies from 55% to 90%.

A. Fluid equations

In our model, we consider the sheath near a rf-biased electrode which is placed at $x=0$ and adopt the one-dimensional configuration. Meanwhile, we assume that the sheath is infinite in the direction parallel to the electrode surface and that the plasma structure is also infinite in the y and z directions.

Under the low pressure condition, due to the sheath thickness being much less than the mean free path of ions and neutral particles, it is reasonable to neglect collisions between ions and neutral particles. Also, we can neglect the ion thermal motion effects since the ion temperature is much smaller than the directional kinetic energy in the sheath region. Thus, the ion dynamics can be modeled using cold ion fluid equations,

$$\frac{\partial n_j}{\partial t}+\frac{\partial(n_j u_j)}{\partial x}=0, \tag{1}$$

$$\frac{\partial u_j}{\partial t}+u_j\frac{du_j}{dx}=-\frac{e}{m_j}\frac{\partial V}{\partial x}, \tag{2}$$

where $n_j(x,t)$, $u_j(x,t)$, and m_j are the ion density, the ion drift velocity, and the ion mass of the jth species ($j=Ar^+$, CF^+, CF_2^+, CF_3^+, and F^-), respectively. In Eq. (2), e is the electronic charge and $V(x,t)$ is the electric potential inside the rf sheath.

The electric potential $V(x,t)$ is determined by Poisson's equation,

$$\frac{\partial^2 V}{\partial x^2}=-\frac{e}{\varepsilon_0}(n_{Ar^+}+n_{CF^+}+n_{CF_2^+}+n_{CF_3^+}-n_e-n_{F^-}), \tag{3}$$

where ε_0 is the permittivity of free space, $n_e(x,t)$ is the electron density. Here we consider that the electron density in the rf sheath change continuously and is given by the Boltzmann distribution,

$$n_e(x,t)=n_0(1-\alpha_{F^-})\exp\left(\frac{eV(x,t)}{k_BT_e}\right), \tag{4}$$

where n_0 is the bulk plasma density, $\alpha_{F^-}=(n_{F^-})_0/n_0$, $(n_{F^-})_0$ is the bulk density of the negative fluorine ion, k_B is the Boltzmann constant, and T_e is the electron temperature.

In present work, we assume that the sheath interface at the time t locates at $x=d_s(t)$ which is the time-dependent sheath thickness. At the sheath boundary, the sum of all positive ion densities should be equal to the sum of the electron and negative fluorine ion density, i.e., the quasineutral condition,

$$n_{Ar^+}(d_s,t)+n_{CF^+}(d_s,t)+n_{CF_2^+}(d_s,t)+n_{CF_3^+}(d_s,t)=n_e(d_s,t)+n_{F^-}(d_s,t). \tag{5}$$

Besides, according to Riemann's work [28], we also assume that the positive ions of the jth species enter the sheath with a velocity equal to the Bohm velocity $u_{jB}=\sqrt{k_BT_e/m_j}$, i.e.,

$$u_j(d_s,t)=u_{jB}. \tag{6}$$

While the negative fluorine ions enter the sheath with a thermal velocity $u_F=\sqrt{k_BT_{F^-}/m_{F^-}}$, where T_{F^-} is the fluorine ion temperature. Finally, we assume that the potential at the sheath edge is approximately zero, i.e.,

$$V(d_s,t)=0, \tag{7}$$

and take the value of the potential at the electrode $(x=0)$ to be

$$V(0,t)=V_e(t), \tag{8}$$

where $V_e(t)$ will be obtained by coupling Eqs. (1)–(3) to a current balance equation, see the following content.

B. Equivalent circuit model of the sheath

Among the above sheath boundary conditions, the time-dependent sheath thickness $d_s(t)$ and the instantaneous voltage $V_e(t)$ on the electrode are unknown quantities. It is well known [2] that although a sinusoidal rf current source is applied on the electrode, the voltage on the electrode is not exactly sinusoidal due to the effects of the sheath loading. In fact, both the forms and amplitudes of the voltage on the electrode should be determined self-consistently by the current balance condition on the electrode, just as the equivalent circuit model [9] with which the relationship between the instantaneous voltage $V_e(t)$ and the sheath thickness $d_s(t)$ can be determined self-consistently. In the equivalent circuit model, the sheath is modeled as a parallel combination of a diode, a capacitor, and a current source. The current through the diode represents the variation of the electron current as a function of the voltage at the electrode,

$$I_e(t)=\frac{eu_e n_0 A}{4}\exp\left(\frac{eV_e(t)}{k_B T_e}\right), \tag{9}$$

where A is the electrode area and $u_e=\sqrt{8k_BT_e/\pi m_e}$ is the mean velocity of an electron with mass m_e.

The current source represents the currents due to the ions incident onto the electrode, which are expressed by

$$I_j(t)=eu_j(0,t)n_j(0,t)A. \tag{10}$$

The current through the capacitor is due to the time variation of the charge Q at the electrode and can be derived as

$$I_d(t)=\frac{dQ}{dt}=\frac{d(C_sV_e)}{dt}=C_s\frac{dV_e}{dt}+V_e\frac{dC_s}{dt}, \tag{11}$$

where $C_s(t)=\varepsilon_0 A/d_s(t)$ is the time-dependent sheath capacitance. Assuming that the rf current applied at the electrode is sinusoidal, we can obtain the current balance equation

$$\sum_j I_j(t)-I_e(t)-C_s(t)\frac{dV_e(t)}{dt}-V_e(t)\frac{dC_s(t)}{dt}=I_{\max}\sin(\omega t), \tag{12}$$

where $I_{\max}$ is the amplitude of the applied rf-bias current and ω is the applied rf frequency. It should be stressed that this current balance equation is also obtained by Edelberg and Aydil [9] for single-ion species sheaths, but they assumed a constant ion current at the electrode and neglected the second term $V_e(dC_s/dt)$ on the right side of Eq. (11). In contrast, considering that the ion dynamics is governed by the instantaneous electric field, we adopt a time-dependent ion current $I_j(t)$ at the electrode. Moreover, the second term $V_e(dC_s/dt)$ is retained in this work in order to make the model fully consistent.

The rf-bias power can be calculated from the time-dependent voltage and the current wave form as follows:

TABLE I. The main parameters in the computation.

Parameter	Notation	Value
Fluorine ion temperature	T_{F^-}	0.067 ev
Ion proportion (Ar^+)	α_{Ar^+}	0.65
Ion proportion (F^-)	α_{F^-}	0.15
Ion proportion (CF^+)	α_{CF^+}	$(1-\alpha_{Ar^+})\times 0.5$
Ion proportion (CF_2^+)	$\alpha_{CF_2^+}$	$(1-\alpha_{Ar^+})\times 0.3$
Ion proportion (CF_3^+)	α_{CF_3}	$(1-\alpha_{Ar^+})\times 0.2$

$$P=\frac{1}{\tau}\int_0^\tau V_e(t)I(t)dt, \tag{13}$$

where $\tau=2\pi/\omega$ is the rf cycle and $I(t)=I_{\max}\sin(\omega t)$. In most experiments, the rf-bias power P is an input parameter. In our calculations, we first choose a value of the amplitude of the rf current $I_{\max}$, then get the wave form of the electrode voltage $V_e(t)$ by solving Eq. (12) and a value of the power P by integrating Eq. (13). Thus, by adjusting the $I_{\max}$ value, the numerical course is repeated until the calculated power equals to the input power we need. Furthermore, for convenience in calculations, we use the Debye length λ_d, the argon ion plasma frequency ω_p, argon ion Bohm velocity u_B, bulk plasma density n_0, and electron temperature k_BT_e/e to nondimensionalize the position x, time t, ion velocity u_j, ion density n_j, and potential V, respectively.

C. Ion energy distributions

The IEDs bombarding the rf-biased electrode can be obtained based on the above model. It should be stressed that this method to calculate the IEDs is suitable only for collisionless sheaths. We know that both the positive ion flux $J=\Sigma_j n_j u_j$ and the positive ion energy $E=\Sigma_j m_j u_j^2/2$ on the electrode at any time in a rf cycle can be obtained with the self-consistent hydrodynamics model of the sheath, shown as before. Therefore, N, the number of positive ion arriving at the electrode in one rf cycle with energy below a certain value E, can be calculated. Thus, the IEDs can be expressed by

$$f(E)=\frac{dN(E)}{dE}. \tag{14}$$

Now we get a set of closed nonlinear equations that determines the spatiotemporal dependence of the rf sheath and the IEDs for multicomponent gas discharges. The above equations with the boundary conditions will be solved numerically in the following section by using a finite difference scheme with an iterative process.

III. RESULTS AND DISCUSSION

In this section, we now present results by solving the hydrodynamics equations and the current balance equation with boundary conditions in a C_4F_8/Ar plasma. The parameters used in the computation are summarized in Table I.

In the following calculations, we find that the negative

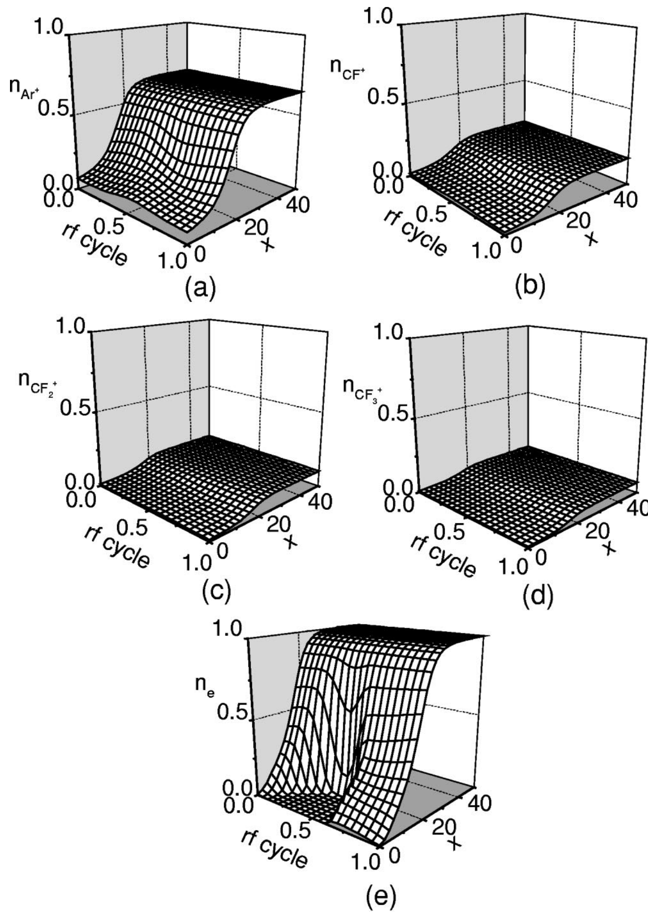

FIG. 1. The spatiotemporal variations of (a) the argon ion density n_{Ar^+} (b) the fluorocarbon ion density n_{CF^+} (c) the fluorocarbon ion density $n_{\mathrm{CF}_2^+}$ (d) the fluorocarbon ion density $n_{\mathrm{CF}_3^+}$, and (e) the electron density n_e in the sheath for $\alpha_{\mathrm{Ar}^+}=0.65$ in a $\mathrm{C_4F_8/Ar}$ plasma. The densities of multiion are all normalized by the bulk plasma density n_0.

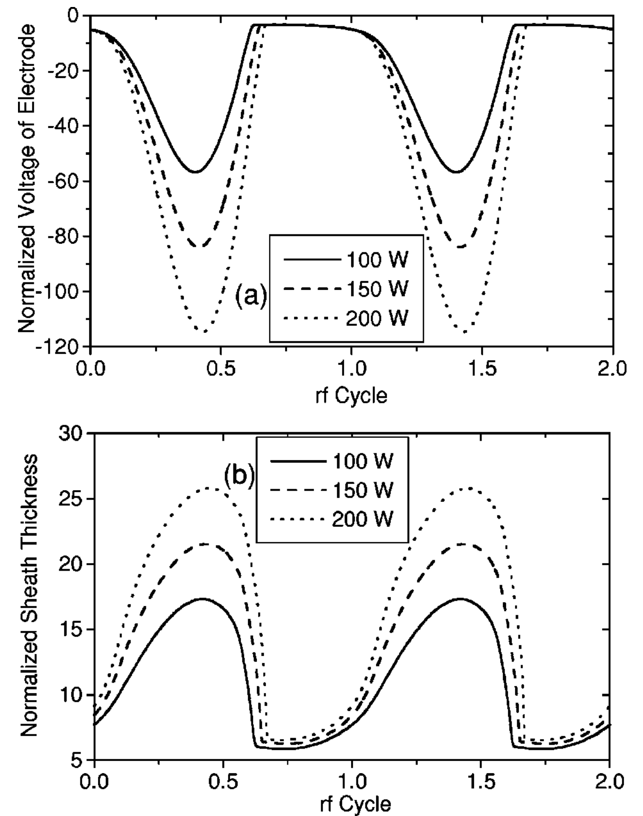

FIG. 2. (a) The instantaneous electrode voltage $V_e(t)$ normalized by the electron temperature k_BT_e/e and (b) the time-dependent sheath thickness $d_s(t)$ normalized by the Debye length λ_d for several rf-bias powers with the rf-bias frequency, the bulk plasma density, and the electron temperature kept constant at 13.56 MHz, $2.0\times10^{11}\ \mathrm{cm}^{-3}$, and 2 eV, respectively.

fluorine ions make very little contribution to the sheath. Actually, the thermal velocity of the fluorine ions is very small because the fluorine ions have heavy mass and low temperature. Additionally, due to the existence of the average negative potential in the sheath, it is very difficult for the negative fluorine ions to overcome the average negative potential and enter into the sheath. Thus, the fluorine ion density n_{F^-} in the sheath is almost zero. Figures 1(a–d) display the spatiotemporal variations of (a) the argon ion density n_{Ar^+}, (b) the fluorocarbon ion density n_{CF^+}, (c) the fluorocarbon ion density $n_{\mathrm{CF}_2^+}$, (d) the fluorocarbon ion density $n_{\mathrm{CF}_3^+}$, and (e) the electron density n_e in the sheath for $\alpha_{\mathrm{Ar}^+}=0.65$, where $\alpha_{\mathrm{Ar}^+}=(n_{\mathrm{Ar}^+})_0/n_0$ and $(n_{\mathrm{Ar}^+})_0$ are the bulk density of the argon ion. The densities of multiion are all normalized by the bulk plasma density n_0 and the distance from the electrode is normalized by the Debye length λ_d. For a rf sheath, the instantaneous potential at the rf-biased electrode can be decomposed into two parts: the first part is the negative dc self-biased voltage and the second part is approximately sinusoidal voltage as shown in Fig. 2(a). Because the negative voltage exists all the time in etching processes, the positive ions will be accelerated toward the electrode impinging onto the substrate. Therefore, all the positive ion densities decrease from the bulk plasma density at the plasma-sheath interface to the electrode. In contrast, electrons are expelled away from the substrate electrode and leave the sheath to the bulk plasma rapidly. Thus, the drop in the electron density is even steeper. Electrons reach the electrode only when the sheath potential drop is small enough and the sheath is thin. This corresponds to the flat regions of the voltage at the electrode shown in Fig. 2(a).

For values of the rf-bias powers and a given frequency $f=13.56$ MHz, the voltage at the rf-biased electrode $V_e(t)$ normalized by the electron temperature k_BT_e/e and the corresponding time-dependent sheath thickness $d_s(t)$ normalized by the Debye length λ_d are also calculated, shown in Figs. 2(a and b), respectively. It is clear that as the potential wave form reaches its maximum voltage drop, the sheath thickness also reaches its maximum.

The time dependence of the positive ion flux $\Sigma_j n_j u_j$ impinging onto the electrode is shown in Fig. 3 for different values of rf-bias frequency. The time t is normalized by the argon ion plasma frequency ω_p. In the low-frequency range ($\beta\ll1$, where $\beta=\omega/\omega_{pj}$, ω_{pj} being the jth species ion plasma frequency) when the rf-bias frequency is less than the ion plasma frequencies of all ion species, the ions cross the

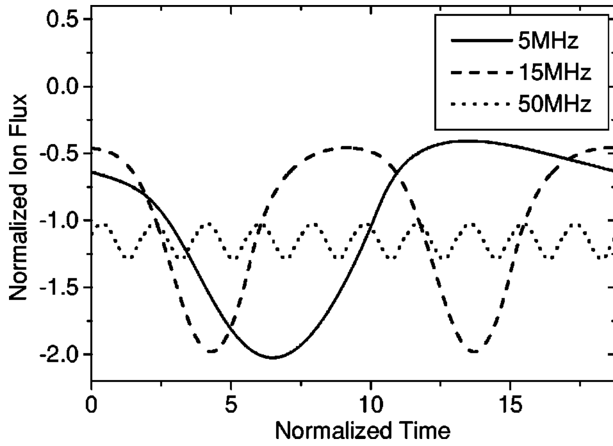

FIG. 3. The time-dependent ion flux $\Sigma_j n_i u_i$ incident onto the rf-biased electrode for different values of the rf-bias frequency with the rf-bias power, the bulk plasma density, and the electron temperature kept constant at 150 W, 2.0×10^{11} cm^{-3}, and 2 eV, respectively.

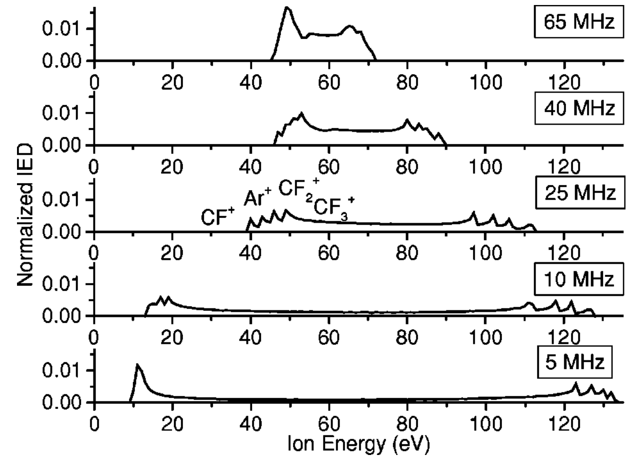

FIG. 4. The effect of the rf-bias frequency on the ion energy distributions with the rf-bias power, the bulk plasma density, and electron temperature kept constant at 150 W, 2.0×10^{11} cm^{-3}, and 2 eV, respectively.

sheath in a small fraction of a rf cycle and respond to the slowly varying instantaneous potential in the sheath. Therefore, the ion flux oscillates strongly and its amplitudes deviate from a constant ion flux significantly. However, in the high-frequency range ($\beta\gg1$), when the applied rf frequency is much higher than the ion plasma frequencies, the ions will take many rf cycles to cross the sheath and can not respond to the instantaneous variation of the rf field due to their inertia. In fact, the ion dynamics is governed by a time-averaged field in the sheath. In the case, the amplitude of the ion flux is very small and almost closes to the constant ion flux. The similar behavior that ion flux oscillates with time in the low- and intermediate-frequency range has been obtained by single-ion species models [12–14]. This shows that it is reasonable to assume a constant ion flux through the sheath only in the high bias frequency in which ions respond to the time-averaged electric field instead of instantaneous sheath electric field.

Figure 4 shows the effect of the rf-bias frequency on the simulated IEDs with the rf-bias power, the bulk plasma density, and the electron temperature kept constant at 150 W, 2.0×10^{11} cm^{-3}, and 2 eV, respectively. For single-ion species rf sheaths, it has been well known from many experiments and simulations [9,14–19,29–31] that the IEDs incident onto the rf-biased electrodes are bimodal. In the present work, therefore, the IEDs also should have the similar bimodal shapes. Indeed, one can observe from Fig. 4 that there are two main peaks in the IEDs, but both the low- and high-energy main peak split into some small peaks. Actually, the peak split results from the existence of multi-ion species, i.e., the ions with different mass correspond to different shapes of the IEDs. The similar phenomenon have been observed by experiments [20,21,29,30,32]. Furthermore, we also observe that as the rf frequency is increased, the peak splits in the high-energy regions will become indistinguishable.

In order to interpret the peak splits, we now consider two parameters. One is the positive ion transit time across the sheath, $\tau_j 2\pi/\omega_{pj}$, and the other is the rf period, $\tau_{rf}=2\pi/\omega$. In the low- and intermediate-frequency range, i.e., $\tau_j/\tau_{rf}\leqslant1$ or $\beta\leqslant1$, the ion transit time τ_j across the sheath is less than or on the order of the rf period and the ion motion responds to the instantaneous sheath voltage. Final energies of the ions depend strongly on the initial phase of the rf cycle in which they enter the sheath and the two peaks in the IEDs correspond to the minimum and maximum sheath drops. Ions traversing the sheath during the period in the rf cycle where the potential drop across the sheath is small will arrive at the electrode with low energies and contribute to the low-energy peak in the IED. In contrast, the ions entering and traversing the sheath during the period in the rf cycle where the potential drop across the sheath is large will arrive at the electrode with high energies and contribute to the high-energy peak in the IED. For multi-ion species plasmas, the transit time for different ion species are different due to their different mass, such as τ_{Ar^+}, τ_{CF^+}, $\tau_{\mathrm{CF}_2^+}$, and $\tau_{\mathrm{CF}_3^+}$. Thus, the energy width of the IED and the height of the two peaks in the IED are different for different ion species, which leads to different shapes of the IEDs, i.e., the peak splits. In the high-frequency range ($\tau_j/\tau_{rf}\gg1$ or $\beta\gg1$), however, the ions take many rf cycles to cross the sheath and only respond to the time-average sheath voltage. In this case, the initial phase when ions enter the sheath becomes unimportant and the ion energy bombarding the substrate is determined by the average sheath potential, which results in a narrow peak in the IEDs for all ion species. Thus, as the rf frequency increases, the energy width of the IED shrinks and the two peaks of the IED approach each other. So in this case, the peak splits in the IEDs become inconspicuous because the difference among the different ion transit time is unimportant.

Figure 5 shows effects of the rf-bias power on the IEDs while keeping the rf-bias frequency, the bulk plasma density, and electron temperature at 13.56 MHz, 2.0×10^{11} cm^{-3}, and 2 eV, respectively. As mentioned in preceding section, the rf-bias power is regarded as an input parameter and the electrode voltage can be determined self-consistently from Eqs. (12) and (13). We find that this calculation method is

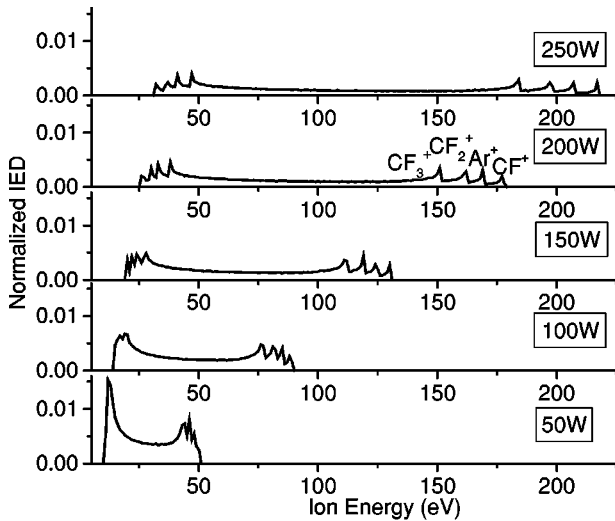

FIG. 5. The effect of the rf-bias power on the ion energy distributions with the rf-bias frequency, the bulk plasma density, and electron temperature kept constant at 13.56 MHz, 2.0×10^{11} cm^{-3}, and 2 eV, respectively.

feasible since the calculated electrode voltages are in the range of operating voltages in practice. For example, if we choose the input power as 50 and 200 W, then corresponding the maximum values of the calculated electrode voltage (normalized by k_BT_e/e) are -27 and -96, respectively. It is can be seen from Fig. 5 that the energy width between the low- and high-energy peak position becomes larger as the rf-bias power is increased. The reason of this is that the peak-to-peak voltage at the electrode is increased with the increasing rf power, as shown in Fig. 2(a). The increasing maximum voltage difference imply that the maximum energy obtained by ions will be much more higher, which leads to a shift of the high-energy peak position to higher-energy region. Accordingly, the energy width of the IED for different ion species is broaden with the increasing rf-bias power, which result in larger energy splits both in the low- and high-energy peak.

Figure 6 display the effects of changing the plasma density on the simulated ion energy distribution while keeping the rf-bias frequency, the rf-bias power, and the electron temperature at 13.56 MHz, 150 W, and 2 eV, respectively. Decreasing the ion density shifts the high-energy peak position of the IED to higher-energy region and makes the peak splits more significant. It is clear from Eq. (12) that changing the plasma density will affect the voltage of the electrode. Similar to the effect of the rf-bias power on the voltage of the electrode, the calculation (not be presented here) also shows that the peak-to-peak voltage increases with the decreasing plasma density and this accounts for that the width between the low- and high-energy peak become large. Therefore, the energy peak splits become significant as the plasma density is decreased.

Finally, we plot effects of the electron temperature on the IEDs in Fig. 7 with the rf-bias frequency, the rf-bias power, and the plasma density held constant at 13.56 MHz, 150 W, and 2.0×10^{11} cm^{-3}, respectively. The effect of decreasing the electron temperature is the increase in energy width between the low- and high-energy peak of the IED. The positions of the high-energy peaks shift to higher-energy region with decreasing electron temperature. Simultaneously, the peak splits in IEDs become wider. Also, it is clear from Eq. (12) that the variation of the electron temperature will lead to the variation of the voltage at the electrode. The calculation (also not be presented here) indicates that the maximum voltage difference between the plasma and the electrode is increasing with the decreasing electron temperature. This results in that the positions of the high-energy peaks shift to a higher-energy region.

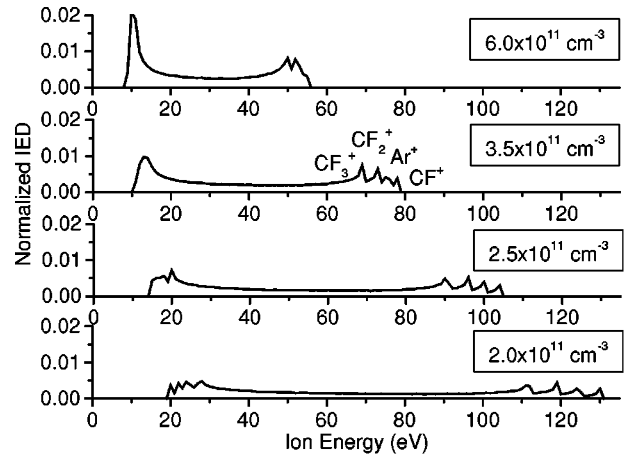

FIG. 6. The effect of the plasma density on the ion energy distributions with the rf-bias frequency, the rf-bias power, and electron temperature kept constant at 13.56 MHz, 150 W, and 2 eV, respectively.

IV. CONCLUSIONS

In the present work, a self-consistent dynamics model of collisionless rf modulated sheaths has been used to predict the rf sheath characteristics and the ion energy distributions impinging on the rf-biased electrodes for multicomponent plasmas. With an equivalent circuit equation, the instanta-

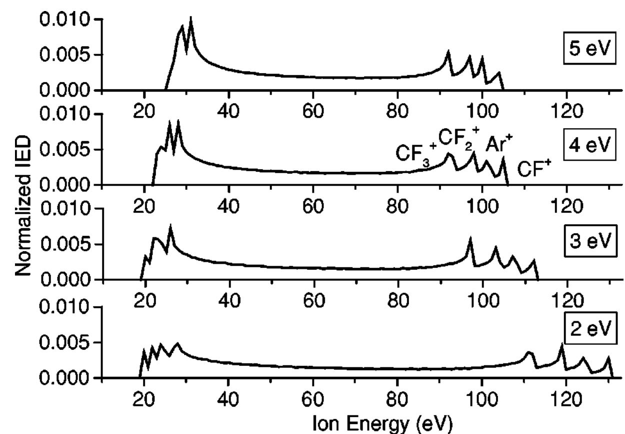

FIG. 7. The effect of the electron temperature on the ion energy distributions with the rf-bias frequency, the rf-bias power, and the bulk plasma density kept constant at 13.56 MHz, 150 W, and 2.0×10^{11} cm^{-3}, respectively.

neous relationship between the sheath voltage and sheath thickness is determined self-consistently. The spatiotemporal variations of different species ion densities, the sheath voltage drop, and the sheath thickness are calculated by including all time-dependent terms in the ion fluid equations. The positive ion densities decrease smoothly from the sheath boundary to the electrode and the negative fluorine ion density in the sheath is almost zero, while the electron density drop fast. The calculated ion energy distributions for the multicomponent plasmas are bimodal, and the width between the low- and high-energy peaks in the IEDs become larger with the increasing bias power or the decreasing bias frequency, bulk plasma density, and electron temperature. In particular, it has been found that the low- or high-energy peaks split into many small peaks due to the existence of ions with different mass. As increasing the rf-bias frequency, the energy splits in the energy peaks become indistinguishable.

The model presented here does not consider collision effects among particles in the sheath and is suitable only for describing sheaths in the low pressure discharge. In the future work, we will extend the present work to include elastic and exchange collisions occurring in the rf sheath and simulate the IEDs and IADs arriving at the rf-biased electrodes with the Monte Carlo method for multicomponent gas discharges.

ACKNOWLEDGMENTS

This work was jointly supported by the National Natural Science Foundation of China (Grant Nos. 19975008 and 19835030) and the Grant for Striding-Century Excellent Scholar of Ministry of Education State of China.

[1] A. Metze, D.W. Ernie, and H.J. Oskam, J. Appl. Phys. **60**, 3081 (1986).
[2] M.A. Lieberman, IEEE Trans. Plasma Sci. **16**, 638 (1988).
[3] M.A. Lieberman, IEEE Trans. Plasma Sci. **17**, 338 (1989).
[4] V.A. Godyak and N. Sternberg, Phys. Rev. A **42**, 2299 (1990).
[5] N. Sternberg and V.A. Godyak, J. Comput. Phys. **111**, 347 (1994).
[6] M.A. Sobolewski, Phys. Rev. E **56**, 1001 (1997).
[7] J. Gierling and K.U. Riemann, J. Appl. Phys. **83**, 3521 (1998).
[8] K.U. Riemann, J. Appl. Phys. **65**, 999 (1989).
[9] E.A. Edelberg and E.S. Aydil, J. Appl. Phys. **86**, 4799 (1999).
[10] P.A. Miller and M.E. Riley, J. Appl. Phys. **82**, 3689 (1997).
[11] T. Panagopoulos and D.J. Economou, J. Appl. Phys. **85**, 3435 (1999).
[12] D. Bose, T.R. Govindan, and M. Meyyappan, J. Appl. Phys. **87**, 7176 (2000).
[13] M.A. Sobolewski, Phys. Rev. E **62**, 8540 (2000).
[14] Z.L. Dai, Y.N. Wang, and T.C. Ma, Phys. Rev. E **65**, 036403 (2002).
[15] P. Benoit-Cattin and L.C. Bernard, J. Appl. Phys. **39**, 5723 (1968).
[16] A. Metze, D.W. Ernie, and H.J. Oskam, J. Appl. Phys. **65**, 993 (1989).
[17] M.J. Kushner, J. Appl. Phys. **58**, 4024 (1985).
[18] M. Misakian and Y. Wang, J. Appl. Phys. **87**, 3646 (2000).
[19] E. Kawamura *et al.*, Plasma Sources Sci. Technol. **8**, R45 (1999).
[20] A.D. Kuypers and H.J. Hopman, J. Appl. Phys. **67**, 1229 (1990).
[21] E.A. Edelberg *et al.*, J. Vac. Sci. Technol. A **17**, 506 (1999).
[22] B.K. Sarma *et al.*, Phys. Lett. A **244**, 127 (1998).
[23] R. Hrach and V. Hrachova, Vacuum **60**, 229 (2001).
[24] H.J. Kim, Surf. Coat. Technol. **112**, 318 (1999).
[25] V. Midha and D.J. Economou, J. Appl. Phys. **90**, 1102 (2001).
[26] K.N. Ostrikov, S. Kumar, and H. Sugai, Phys. Plasmas **8**, 3490 (2001).
[27] K. Teii *et al.*, J. Vac. Sci. Technol. A **18**, 1 (2000).
[28] K.U. Riemann, Phys. Fluids B **4**, 2693 (1992).
[29] A.D. Kuypers and H.J. Hopman, J. Appl. Phys. **63**, 1894 (1988).
[30] A. Manenschijn *et al.*, J. Appl. Phys. **69**, 1253 (1991).
[31] C. Charles *et al.*, Phys. Plasmas **7**, 5232 (2000).
[32] N. Mizutani and T. Hayashi, Thin Solid Films **374**, 167 (2000).